01 Apr 2022

# 2-D Tilt Sensor based on Coaxial Cable Fabry-Perot Resonators with Submicroradian Resolution

Chen Zhu
*Missouri University of Science and Technology*, cznwq@mst.edu

Yan Tang

Yiyang Zhuang

Jing Guo

*et. al. For a complete list of authors, see https://scholarsmine.mst.edu/ele_comeng_facwork/4724*



## Recommended Citation

C. Zhu et al., "2-D Tilt Sensor based on Coaxial Cable Fabry-Perot Resonators with Submicroradian Resolution," *IEEE Transactions on Microwave Theory and Techniques*, vol. 70, no. 4, pp. 2398 - 2406, Institute of Electrical and Electronics Engineers, Apr 2022.
The definitive version is available at https://doi.org/10.1109/TMTT.2021.3136555

# 2-D Tilt Sensor Based on Coaxial Cable Fabry–Perot Resonators With Submicroradian Resolution

Chen Zhu, *Member, IEEE*, Yan Tang, Yiyang Zhuang, Jing Guo, Rex E. Gerald II, and Jie Huang, *Senior Member, IEEE*

***Abstract*— For the past 50 years, open-ended coaxial lines were commonly employed for the determination of electromagnetic properties of various materials. In this article, the application of an open-ended hollow coaxial cable resonator (OE-HCCR) as a 1-D inclinometer for tilt measurements with 110 nanoradian (nrad) resolution is proposed and demonstrated. The coaxial cable resonant structure is formed between a metal post welded within the coaxial cable at the RF input end and the open end of the coaxial cable. A metal mass block, suspended in proximity to the open end in parallel is used to construct a pendulum structure, serving as the element responsive to a tilt. When the device is tilted, the distance between the mass block and the open end varies due to the displacement of the suspended pendulum. The change in the gap distance modifies the phase reflection coefficient associated with the open end, causing the resonance frequency of the coaxial cable resonator to change. By tracking the resonance frequency, the coaxial line resonator is effectively used as an inclinometer. The experimental results demonstrated that the novel device has a measurement resolution of 110 nrad over a range of 0–3 milliradians (mrad). Additionally, based on the same principle, a 2-D inclinometer based on two perpendicularly aligned OE-HCCRs, useful for simultaneous tilt measurements in two orthogonal dimensions is demonstrated. The open-ended coaxial cable resonator-based inclinometer holds several advantages, including high resolution, robustness, cost effectiveness, ease of signal interrogation, and user-configurable sensitivity and dynamic range.**

***Index Terms*— Coaxial cable device, microwave sensor, open-ended coaxial cable resonator, tilt sensor, 2-D inclinometer.**

## I. Introduction

TILT measurements are of great significance in structural health monitoring (SHM), prediction of natural disasters such as landslides and earthquakes, detection of gravitational waves, and in studies of solid tides [1]–[3]. A pendulum is typically employed as the tilt-sensitive element in traditional inclinometers. Various methods have been developed to monitor the tilt-induced movement of the pendulum [4], [5]. In recent years, fiber-optic inclinometers have been vigorously studied and reported because they offer unique features, including lightweight, small size, immunity to electromagnetic interference, harsh environment survivability, and remote operation capability [6]–[8]. The majority of the reported fiber-optic inclinometers are based on fiber Bragg gratings (FBGs). In FBG-based inclinometers, the tilt is transferred to the strain applied to an FBG or multiple FBGs. The applied strains lead to shifts in the resonance wavelength of the FBGs [9]–[12]. The FBG inclinometers have shown wide dynamic measurement ranges. However, the measurement resolution is limited to around 17.5 $\mu$rad due to the strain transfer-based working principle of this type of inclinometer [11]. Other types of fiber-optic inclinometers have also been reported, including some based on Michelson interferometers [13], [14]. These inclinometers work by bending a sensor structure, where the tilt is transferred to the bending angle of the sensor head. The bending structure approach inevitably and significantly degrades the robustness and durability of the sensors. Also, the measurement resolution is limited to 20 $\mu$rad [13]. Recently, an optical extrinsic Fabry–Perot interferometer (EFPI) based inclinometer with the ultrahigh resolution was demonstrated [15]. A two-rope suspended pendulum structure was used as the tilt-sensitive element in the sensor design, and an optical inteferometer was used to meter the movement of the pendulum that was subject to a tilt. However, the fabrication process of this sensor was complicated, and the signal interrogation unit was costly.

In recent years, researchers have been exploring coaxial cable sensor devices mimicking their optical fiber counterparts [16]. Examples include the coaxial cable Bragg grating (CCBG) [17], [18], the coaxial cable Fabry–Perot interferometer (CCFPI) [19], and the hollow coaxial cable Fabry–Perot resonator (HCC-FPR) [20]–[24]. The CCBG and CCFPI were employed for measurements of large strains, up to 5%. The HCC-FPRs were successfully used for measurements of displacement and strains in high-temperature environments, up to 1000 °C [22], and for wide-range and high-resolution liquid level monitoring [21]. Preliminary explorations revealed that coaxial cable sensors could provide a viable solution for some challenging issues faced by fiber-optic sensors in specific scenarios, such as SHM and harsh-environment applications that involve heavy-duty use, large strains, and elevated temperatures. Therefore, the development of coaxial cable sensor devices needs to be continued and advanced further.

Open-ended coaxial lines have been employed over the past 50 years for the determination of electromagnetic prop-

Manuscript received September 13, 2021; revised November 13, 2021 and December 6, 2021; accepted December 10, 2021. Date of publication January 4, 2022; date of current version April 4, 2022. *(Corresponding authors: Chen Zhu; Jie Huang.)*

The authors are with the Department of Electrical and Computer Engineering, Missouri University of Science and Technology, Rolla, MO 65409 USA (e-mail: cznwq@mst.edu; jieh@mst.edu).

Color versions of one or more figures in this article are available at https://doi.org/10.1109/TMTT.2021.3136555.

Digital Object Identifier 10.1109/TMTT.2021.3136555

erties of dielectric materials, exhibiting high sensitivity and nondestructive working modalities [25]–[34]. The fundamental operating principle of open-ended coaxial probes is based on the interaction of the fringing electric field with the electromagnetic properties of the material (e.g., in the liquid or solid phase) placed near the open end. Open-ended coaxial line resonators were also employed for complex permittivity measurements [35]–[37]. However, the majority of the reported open-ended coaxial sensors were based on correlating the parameters of interest (e.g., humidity [38] and gas concentration [39]) to dielectric measurements, limiting the applications for coaxial cable sensor devices.

Very recently, a novel sensing scheme, based on an open-ended coaxial line resonator, for probing 1-D displacements with nanometer resolution was reported [40], [41]. In this article, we report on the development of a novel microwave 1-D tilt sensor capable of measuring tiny changes in tilt angles as small as 110 nrad, based on an open-ended hollow coaxial cable resonator (OE-HCCR). The tilt sensing is achieved by using the OE-HCCR to measure the movement of a two-rope suspended metal mass block caused by changes in tilt angles. Taking advantage of the ultrasensitive region provided by the OE-HCCR sensing scheme, the present tilt sensor shows an unprecedented resolution among microwave sensors, as high as 110 nrad. The concept of the 1-D tilt sensor is then extended to a 2-D device, from which a 2-D tilt sensor with high sensitivity is also demonstrated. This report significantly extends our previous work [41] by expanding the OE-HCCR scheme to another milestone for developing microwave sensors that can be potentially used in industrial and scientific applications. The resultant compact 1-D and 2-D tilt sensors provide ultrahigh sensitivity and resolution, and can serve as alternatives to conventional bulky tilt sensors in high-precision measurement and instrumentation fields. Additionally, this work opens a new dimension of applications for open-ended coaxial probes that have been conventionally used for dielectric spectroscopy and material characterization.

Article organization is as follows. The device physics is discussed in Section II. A judicious experiment for demonstrating the high measurement resolution of the device was designed and the results are presented in Section III. Section IV concludes this work.

## II. Sensor Design and Measurement Principle

### A. 1-D Tilt Sensor Design

Schematic of the proposed 1-D inclinometer and a photograph of a prototype device are presented in Fig. 1. Fig. 1(a) shows a schematic of the OE-HCCR-based inclinometer in the orientation with a zero-tilt angle. The sensor device was packaged in an aluminum alloy box, as shown in Fig. 1(b). A homemade all-stainless-steel HCC was used as the sensing platform, which offers high mechanical strength and ease of modification. The traditional dielectric insulator layer (e.g., polyethylene) was removed. The radii of the inner conductor and the outer conductor of the HCC were designed to be 3 and 7 mm, respectively, resulting in a characteristic impedance of 50.8 Ω for air as the dielectric medium. Moreover, the coaxial line design also made the input end of the HCC compatible with a standard n-type connector so that the HCC could be connected to a commercial coaxial cable (e.g., RG-58/U) via a standard SubMiniature version A (SMA) to the n-type adapter. A resonant structure was fabricated from the HCC. A metal post, which was welded near the RF input end, shorts the inner conductor and the outer conductor, serving as the first reflector; the open end of the HCC served as the second reflector. The cavity length of the OE-HCCR

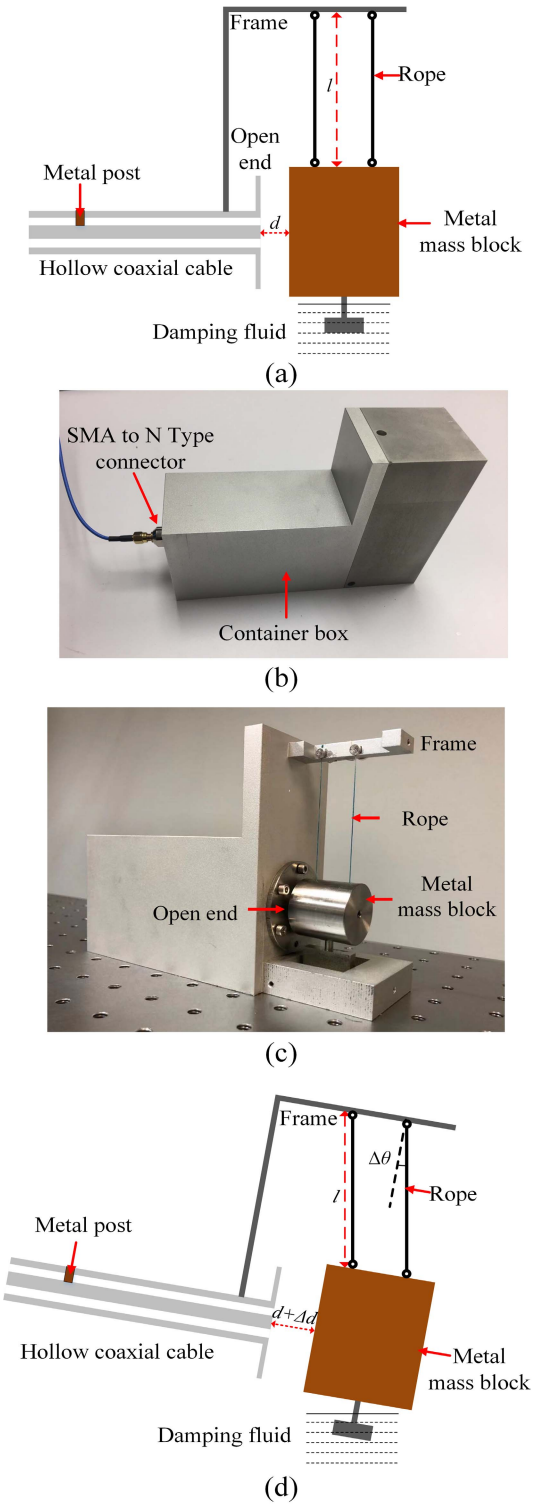


Fig. 1. Schematic of the proposed 1-D inclinometer and photographs of a prototype inclinometer device. (a) Schematic of the side view of the 1-D OE-HCCR-based inclinometer for a zero tilt angle. (b) Photograph of a prototype sensor device packaged in an aluminum alloy box. (c) Detailed view of the prototype sensor. (d) Schematic drawing showing the pendulum-based inclinometer tilted at a positive tilt angle $\Delta\theta$.

(i.e., the distance between the metal post and the open end) was approximately 75 mm. A metal mass block pendulum made of stainless steel was suspended in proximity to the open end. The metal mass block (in the shape of a cylinder) was flexibly connected to the top of the frame using two nylon multistrand ropes with the same lengths. The diameter and length of the cylindrical metal mass block were both 30 mm. The four connection points [i.e., the four eyelets as shown in Fig. 1(a)] were contained in a common plane, defining a rectangle at the zero-tilt setting (i.e., no tilt applied). Note that the frame is part of the container box, and a through-hole was drilled into the side of the container box to accommodate the horizontally oriented OE-HCCR. A detailed view of the prototype sensor is given in Fig. 1(c). As a result, the endface of the mass block maintains a disposition parallel to the open end of the OE-HCCR. When the container box (i.e., the sensor device) is tilted at an angle $\Delta\theta$, as shown in Fig. 1(d), the two ropes remain perpendicular to the horizontal ground plane due to the action of gravity on the mass block. Notably, the mass block remains parallel to the frame due to the parallelogram structure defined by the two perpendicular ropes and the four connection point eyelets. As a result, the gap distance between the open end and the adjacent endface of the metal block changes by $\Delta d$. Note that an oscillation dampening structure was also considered in the sensor design, in which the mass block was connected to a cross paddle immersed in a damping fluid. The dampening structure effectively reduced the vibrations induced by environmental factors. According to the geometric relationships, the tilt angle of the sensor device is given by

$$\Delta\theta = \arcsin\frac{\Delta d}{l} \tag{1}$$

where $l$ is the lengths of the two nylon ropes. Note that in this article, the tilt angle, as shown in Fig. 1(d), is defined as a positive angle. Based on the judicious mechanical design, the tilt angle is directly correlated with the gap distance between the mass block and the open end, $d$. The relationship between the tilt angle and the change in the gap distance is uniquely determined by the lengths of the two ropes. That is, the lengths of the ropes determine the performance parameters of the inclinometer. In general, the longer the ropes, the higher the measurement sensitivity and resolution. However, the dynamic range for the tilt angles is correspondingly sacrificed. Note that in the sensor assembly, the slight misalignment of the mass block and the length discrepancy of the two ropes could result in an unparallel relationship between the metal mass block and the open end of the coaxial line. However, these errors do not affect the performance of the sensor within a small dynamic range (e.g., 0.1 rad in tilt angle) and can be minimized after proper sensor calibration.

### *B. Measurement Principle*

As discussed earlier, a resonating structure was engineered from a basic HCC, consisting of two reflectors, i.e., the metal post and the open endface of the coaxial line. The resonance frequency of the coaxial line resonator is a function of the physical length between the two reflectors and the phase reflection coefficients of the two reflectors. Due to the fringing field excited by the transverse electromagnetic wave traveling in the HCC, the reflection coefficient of the open end is dependent on the distance between the open end and the adjacent endface of the mass block, i.e., $d$. To be specific, the static capacitance at the open end due to the fringing electric field is a function of $d$. When $d$ changes, the capacitance at the open end varies, resulting in a change in the phase reflection coefficient of the open end. The change in the phase reflection coefficient of the open end leads to a shift in the resonance frequency ($f_{\text{res}}$) of the coaxial cable resonator codified by

$$f_{\text{res}} = \frac{c(2m\pi + \phi_1 + \phi_2)}{4\pi L} \tag{2}$$

where $c$ is the speed of light in vacuum; $m$ is an integer, representing the resonance order; $\phi_1$ and $\phi_2$ are the phase reflection coefficients of the metal post and the open end, respectively; and, $L$ is the distance between the metal post and the open end of the coaxial cable. Note that $\phi_1$ and $\phi_2$ are both functions of frequency. Therefore, (2) has no analytical solution. Detailed numerical studies of (2) can be found in our recent work [41]. Fig. 2 briefly presents the numerical investigations of selected reflection and resonance frequency characteristics of the OE-HCCR. Fig. 2(a) shows a typical reflection spectrum of the OE-HCCR calculated based on the numerical model developed in [41]. The reflection spectrum obtained from the full-wave simulation using ANSYS HFSS is also included for comparison. Discrete resonance frequencies can be observed, including the fundamental resonance and several high-order harmonics. The overall trend of reflection spectra obtained from the numerical calculation and full-wave simulation, including the resonance frequencies and the corresponding resonance depths, matches well. Discrepancies can also be observed, revealing the modeling errors. The dependence of the fundamental resonance frequency of the resonator on the distance between the open end of the coaxial cable and the adjacent endface of the mass block $d$ is plotted in Fig. 2(b). The inset in Fig. 2(b) shows an enlarged view for the distance $d$ ranging from 0.1 to 2 mm. The resonance frequency decreases exponentially as $d$ decreases. When $d$ decreases down to 0.1 mm, the OE-HCCR provides a displacement sensitivity that is comparable to a fiber-optic EFPI, which can typically resolve cavity length changes to 1 nm [41]. The resonance frequency of the OE-HCCR has little dependence upon $d$ when it exceeds 10 mm, thus limiting the dynamic range of the inclinometer to 0.125 rad (~7.2°) for

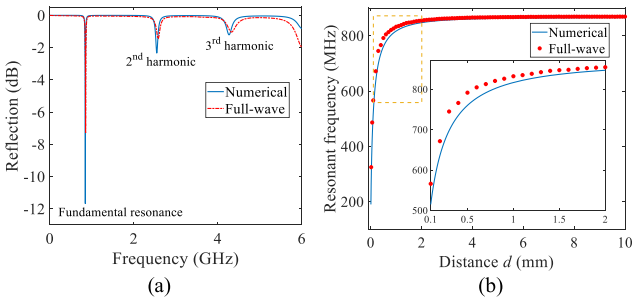


Fig. 2. Numerical investigations and full-wave simulations of selected reflection and resonance frequency characteristics of the OE-HCCR. (a) Reflection spectrum when the gap distance between the open end and the mass block was set to 2 mm. Three resonance dips can be observed, corresponding to the fundamental resonance (~0.847 GHz), the second-order harmonic (~2.549 GHz), and the third-order harmonic (~4.269 GHz). (b) Dependence of the fundamental resonance frequency on the gap distance $d$ between the open end of the coaxial cable and the adjacent endface of the mass block. The inset is an expanded view of resonance frequency versus gap distance for the gap distance range of 0.1 to 2 mm.

a practical rope length of 80 mm. Again, the results obtained from full-wave simulations are also included in Fig. 2(b) for comparison. Noticeable differences of approximately 3% between the calculation and the simulation results can be observed mainly due to the approximation errors introduced in the numerical modeling. However, the evolution of the characteristic curves agrees well, validating the effectiveness of the model. The numerical calculation is more efficient in predicting the response of the OE-HCCR with reasonable accuracy, compared to the full-wave simulation.

In the numerical calculations, the physical length between the metal post and the open end was set to 75 mm. Note that in the sensor design, we tried to lower down the operating frequency of the sensor so that the system cost of the interrogator could be reduced. A low resonance frequency indicates a large resonant cavity, corresponding to a large sensor size. On the other hand, the higher the resonance frequency is, the higher the measurement sensitivity will be, and potentially the higher measurement resolution. Therefore, there is a tradeoff between the size of the resonator (i.e., sensor size), the operating frequency, and the measurement sensitivity and resolution. As a result, we designed the length of the resonant cavity to be 75 mm, and the resultant fundamental resonance frequency was approximately 800 MHz, which also provided the tilt sensor with a satisfactory resolution of submicroradian, as shown later.

Combining the pendulum-based tilt sensing structure that translates variations of tilt angles to changes in gap distances between the mass block and the open end, and the great dependence of the OE-HCCR on the gap distance $d$, a novel high-resolution inclinometer is revealed. Interestingly, the dynamic range and measurement sensitivity (resonance frequency shift/tilt angle change) of the inclinometer is user-configurable. To be specific, as can be seen from Fig. 2(b), the rate of decrease in the resonance frequency keeps increasing as $d$ decreases. As a result, the measurement sensitivity of the inclinometer is dependent on the initial gap distance $d$ between the mass block and the open end; the smaller the gap distance, the higher the sensitivity. This unique feature makes the OE-HCCR-based inclinometer a good candidate for specific applications where the dynamic range and sensitivity for tilt measurements need to be considered. For example, for applications that require small dynamic ranges, such as studying solid Earth tides, the initial gap distance can be set to less than 0.1 mm to achieve ultrahigh sensitivity and resolution (greater than 20 nrad in theory) for a dynamic range of 1.25 mrad (∼0.072°), given the length of the ropes to be 80 mm. Additionally, as shown in (1), the sensitivity and dynamic range of the OE-HCCR-based inclinometer can also be adjusted by changing the length of the ropes.

It is worth mentioning that variations of environmental temperature could have a detrimental impact on the measurement uncertainty of the tilt sensor. When the environmental temperature fluctuates, thermal expansions/contractions will cause changes in the size of the mass block, the container box, and the ropes that are used to suspend the mass block. Consequently, changes in the dimensional size of the individual components will cause variations of the gap distance between the mass block and the open end of the coaxial line, leading to temperature crosstalk of the tilt sensor. However, the contributing effects from the mass block and the container box will partially offset each other. Based on the geometrical structure of the sensor, an estimation of the change in the gap

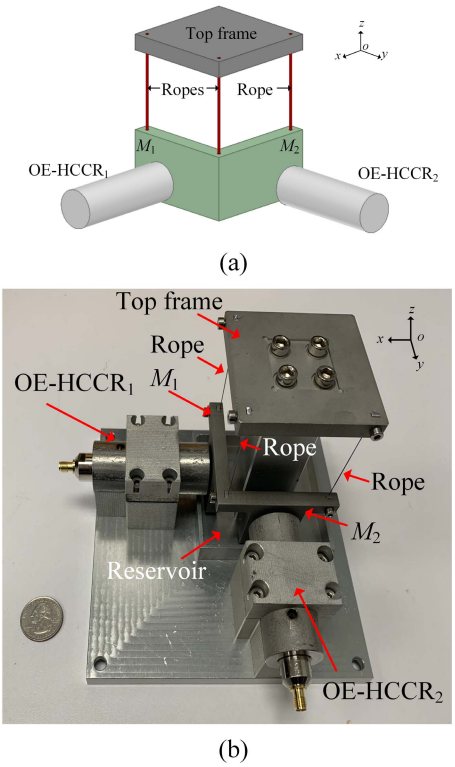


Fig. 3. Schematic and photograph of the proposed 2-D inclinometer device based on two OE-HCCRs and an L-shaped metal bar. (a) Illustration of the 2-D OE-HCCR-based inclinometer. (b) Photograph of a prototype 2-D inclinometer. The two OE-HCCRs and the top frame were mounted to a common metal base.

distance ($\Delta d_T$) caused by a change in temperature ($\Delta T$) is given by

$$\Delta d_T = (d\alpha_{\mathrm{CTE1}} + l\Delta\theta\alpha_{\mathrm{CTE2}})\Delta T \approx d\alpha_{\mathrm{CTE1}}\Delta T \qquad (3)$$

where $\alpha_{\mathrm{CTE1}}$ and $\alpha_{\mathrm{CTE2}}$ represent the coefficient of thermal expansion (CTE) of aluminum alloy and nylon, respectively. For example, a variation of 1 °C in temperature could lead to a change of 3.9 nm in the gap distance, given the CTE of aluminum alloy to be $13 \times 10^{-6}$/°C. Considering the length of the rope to be 80 mm, a variation of 1 °C in temperature yields a change of 49 nrad in tilt angle. Thus, environmental temperature variations could be a possible and significant source of error in the measurement accuracy using the tilt sensor. Therefore, in practical applications, the tilt sensor must be protected in a thermal insulation device to minimize measurement errors caused by temperature crosstalk of the sensor as well as variations of other environmental factors such as humidity. On the other hand, the temperature crosstalk of the tilt sensor can be reduced by selecting different materials for the metal mass block and the frame [see Fig. 1(a)] and combining them with a judicious structural design.

### *C. 2-D Tilt Sensor Design*

Based on the 1-D sensor design and the working principle discussed in Sections II-A and II-B, a 2-D inclinometer for tilt measurements in two orthogonal dimensions, as presented in Fig. 3, is proposed. The principal idea was to use a pair of perpendicularly arranged OE-HCCR and an L-shaped metal bar (with a 90° corner angle) serving as the 2-D tilt sensitive

element, as schematically illustrated in Fig. 3(a). The L-shaped metal bar was suspended from the top frame by three nylon multistrand ropes with the same lengths. The side face $M_1$ of the metal bar was aligned parallel to the open end of OE-HCCR$_1$; the other side face $M_2$ of the metal bar was consequently parallel to the open end of OE-HCCR$_2$. Separately, each OE-HCCR paired with its corresponding metal bar was a high-resolution 1-D inclinometer. The integrated orthogonal design minimized crosstalk errors such that tilt in one of the two orthogonal directions could be unambiguously determined. Ideally, when there is tilt applied along the $x$-axis direction (according to the Cartesian coordinate system shown in the figure), the gap distance between the open end of OE-HCCR$_1$ and side face $M_1$ will change due to the mechanical design, as discussed in Section II-A. The gap distance between the open end of OE-HCCR$_2$ and side face $M_2$ remains constant because of the orthogonal arrangements of OE-HCCR$_2$ and side face $M_2$. Similarly, the gap distance between the open end of OE-HCCR$_2$ and side face $M_2$ will vary when tilt is applied along the $y$-axis direction, whereas the gap distance between the open end of OE-HCCR$_1$ and side face $M_1$ remains unchanged. Fig. 3(b) shows a photograph of a prototype 2-D tilt sensor device. The OE-HCCRs and the top frame were mounted on a common base, where a reservoir was also included. The reservoir was employed for damping fluid, which could physically reduce the deleterious effect of vibrations from the environment, thereby increasing the stability of the inclinometer. The length of each of the three ropes was approximately 60 mm. The cavity lengths of the OE-HCCRs (i.e., the physical distance between the metal post and the open end of the coaxial cable) were approximately 50 mm. The initial gap distance between the open end of the OE-HCCR and the corresponding side face of the metal bar can be precisely set by mechanically adjusting the positions of the OE-HCCRs.

## III. Experimental Results and Discussion

### A. 1-D Tilt Sensor

The dynamic range of the OE-HCCR-based inclinometer was demonstrated first. The lengths of the two ropes were both 80 mm, and the initial gap distance between the endface of the mass block and the open end was set to approximately 1.6 mm (measured using a caliper). The experimental results are presented in Fig. 4. In the experiment, the prototype sensor device was placed on a 1-D tilt translation stage. The resolution and dynamic range of the stage were approximately 293 $\mu$rad ($\sim$0.0168°) and $-0.174$ rad ($-10°$) to 0.174 rad (10°), respectively. A vector network analyzer (VNA, Agilent 8753ES) was used as the signal interrogation unit. The sensor was connected to Port 1 of the VNA via a commercial flexible coaxial cable. Olive oil was used as the damping fluid for the inclinometer. All the experiments were performed at room temperature (25 °C $\pm$ 0.5 °C), normal pressure, and humidity of 40%.

Fig. 4(a) and (b) present the recorded reflection spectra of the inclinometer when tilted to positive and negative angles, respectively. As the tilt angle decreased, the gap distance $d$ between the open end and the mass block decreased, leading to the resonance spectrum shifting to the left (lower resonance frequency), as expected. A Gaussian curve fit was applied to each measured reflection spectrum near its resonance dip, and the best-fitted model was acquired by evaluating the goodness of fit. The resonance frequency was then determined by finding the datapoint in the best-fitted curve where the derivative approached zero. The obtained fundamental resonance frequency of the device as a function of the applied

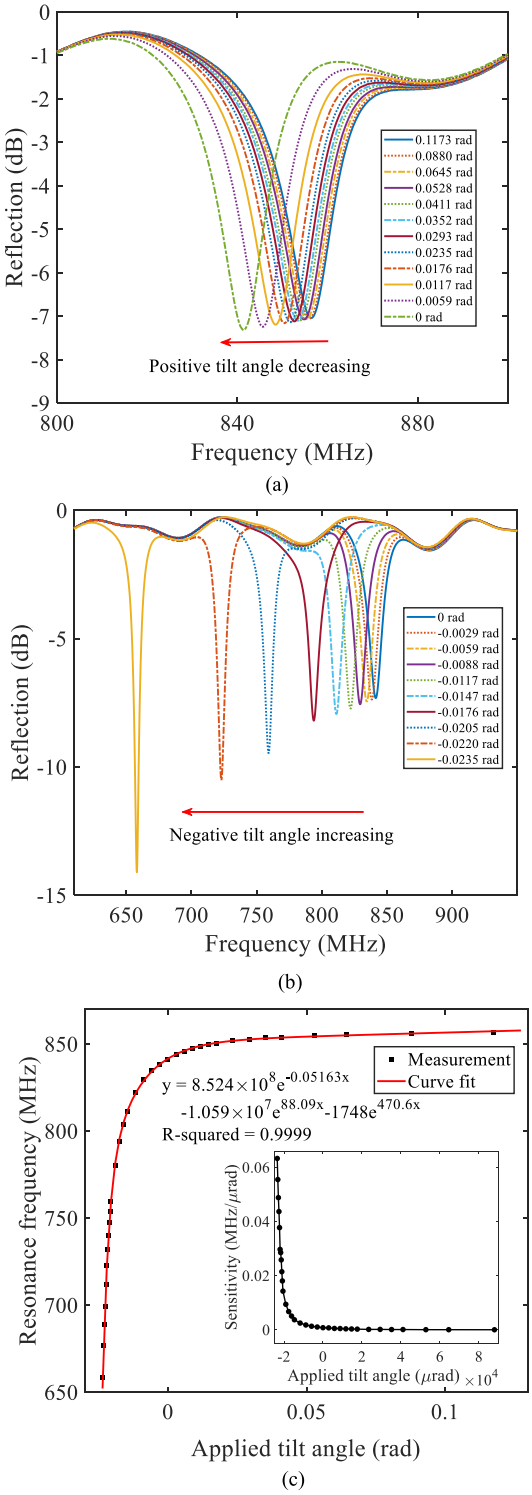


Fig. 4. Responses of the prototype 1-D inclinometer device to a large range variation of applied tilt angles. (a) Recorded reflection spectra of the inclinometer device sensor when tilted to positive angles. (b) Recorded reflection spectra of the device when tilted to negative angles. (c) Measured resonance frequency of the prototype inclinometer as a function of applied tilt angle ranging from $-0.0235$ to 0.1173 rad. The solid red line represents an exponential curve fit to the data points. The inset shows the sensor sensitivity with respect to the applied tilt angle.

tilt angle is shown in Fig. 4(c). Using an exponential model, a curve-fitted equation with an $R$-squared of 0.9999 was obtained, as indicated in Fig. 4(c). As a result, in practice, the measured tilt angle can be obtained by feeding the measured resonance frequency into the curve-fitted equation. For example, for a measured resonance frequency of 803.6 MHz, the measured tilt angle was estimated to be −0.01617 rad, which indicates a 0.2% error compared to the actual value of −0.01614 rad. Note that the error was introduced mainly by the sensor calibration approach, i.e., the exponential curve fit. More advanced sensor calibration techniques, e.g., machine learning techniques, can be employed to reduce the errors.

Based on (1), as the tilt angle applied to the sensor device changed from 0.1173 to −0.0235 rad, the gap distance between the endface of the mass block and the open end decreased in a quasi-linear behavior. The decreases in the gap distance consequently led to exponential decreases of the resonance frequency, as predicted by Fig. 2(b). The exponential trend obtained in Fig. 4(c) matched well with the calculated results shown in Fig. 2(b). The resonance frequency at 0 rad (i.e., no tilt applied) was determined to be 841.3 MHz. Thus, the initial gap distance between the endface of the mass block and the open end was determined to be approximately 1.681 mm, according to Fig. 2(b), close to the set value of 1.6 mm. The inset in Fig. 4(c) shows the measured sensitivity of the sensor (obtained by differentiating the resonance frequency with respect to the applied tilt angle) as a function of the applied tilt angle. The sensor's sensitivity changed rapidly in different tilt angle regions. The experimental results demonstrated that the OE-HCCR device could be used as a sensor for positive and negative tilt angle measurements with a satisfactory dynamic range.

The measurement resolution of the OE-HCCR inclinometer was subsequently investigated. The experiment setup and the responses of the prototype inclinometer are presented in Fig. 5. Fig. 5(a) shows a schematic of the experiment setup employed to demonstrate the measurement resolution of the prototype inclinometer. A steel plain square tube was used as a supporting beam with dimensions 925.0 mm × 25.0 mm × 25.0 mm. The inclinometer was aligned and placed on the left end of the supporting beam. The left end of the beam was constrained by a prism-shaped metal stop, which was mounted to an optical table. The right end of the beam was vertically positioned by a translation stage, offering a vertical displacement resolution of 10 $\mu$m. When a displacement was applied to the free end of the beam along the vertical direction indicated in Fig. 5(a), the supporting beam was tilted with a negative angle. Therefore, the inclinometer was also tilted with the same angle. In the experiment, displacements were applied to the supporting square cross-section tube (beam) by the translation stage in the range 0–400 $\mu$m in steps of 50 $\mu$m, corresponding to a 432 $\mu$rad change in tilt angle implemented in steps of 54 $\mu$rad. Note that before the experiment, the resonance frequency of the inclinometer was tuned to approximately 700 MHz (where the gap distance $d$ between the mass block and the open end was approximately 0.300 mm) to achieve high measurement sensitivity. Pre-tilting of the device to an initial angle was realized by simply applying displacements along the vertical direction to the supporting beam. Fig. 5(b) presents the recorded spectra obtained from the inclinometer. The reflection spectrum shifted to the lower frequency region as the negative

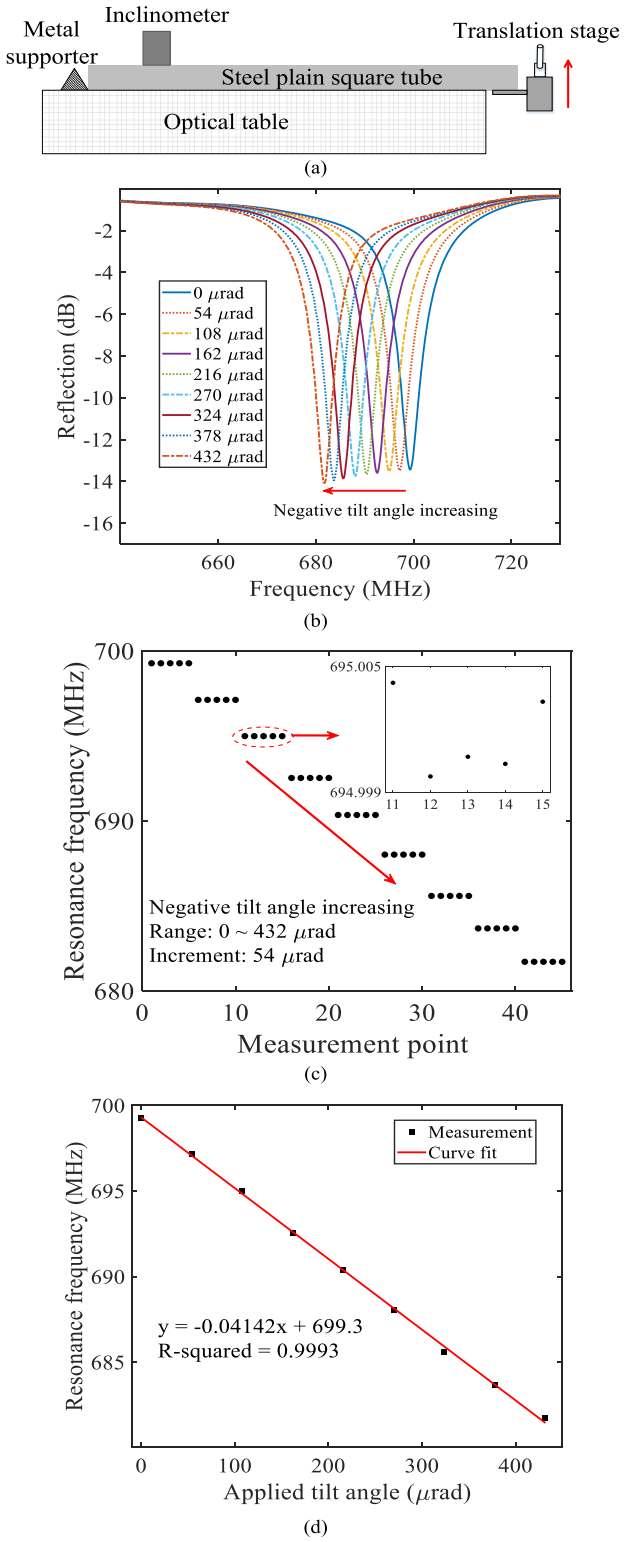


Fig. 5. Investigations of the measurement resolution of the OE-HCCR-based inclinometer device. (a) Schematic of the experiment setup designed to demonstrate the high resolution of the OE-HCCR-based inclinometer device. (b) Recorded reflection spectra of the prototype device for a series of negative tilt angles. (c) Responses of the inclinometer to small changes in applied negative tilt angles. Five measurements were recorded for each tilt angle setting. The inset shows the maximum deviation of the resonance frequency obtained in the experiment. (d) Resonance frequency as a function of negative tilt angle in the range 0–432 $\mu$rad. A linear curve fit was applied to the data, as depicted by the solid-red curve.

tilt angle increased, which matched well with Fig. 4(b). Five measurements for each setting of displacement/tilt angle were recorded. As can be seen from the stair plot in Fig. 5(c), the inclinometer responded well to small changes in tilt angles. The inset shows the maximum deviation of the resonance frequency obtained in the experiment. The maximum deviation was determined to be 4.538 kHz. The measured resonance frequency of the OE-HCCR as a function of applied tilt angle in the range 0–432 $\mu$rad is plotted in Fig. 5(d). A linear curve fit was applied to the data, and a satisfactory linear relationship was obtained with an R-square of 0.9993. The measurement sensitivity (i.e., the slope of the fitted curve) was determined to be 0.04142 MHz/$\mu$rad (41.42 GHz/rad). The sensitivity also matched well with Fig. 4(c). Considering the maximum deviation obtained in the experiment [see Fig. 5(c)], i.e., 4.538 kHz, the tilt measurement uncertainty of the inclinometer at the current laboratory setting was calculated to be 110 nrad over a dynamic range of 3.75 mrad. The measurement uncertainty is due to environmental perturbations such as temperature fluctuations, air flows, experimental setup vibrations, etc., as well as the system noise and uncertainty introduced in the data processing. It is expected that the measurement sensitivity and resolution can be further increased by decreasing the gap distance between the open end and the mass block. The linear curve fit results indicated that the response curve of the inclinometer could be considered as a linear function, if changes in tilt angles are small, e.g., in the range of 0–1 mrad.

It is worth mentioning that as the tilt angle approaches the positive angle region, the sensitivity of the sensor decreases rapidly as shown in the inset of Fig. 4(c). The decrease in sensitivity leads to high uncertainty in tilt angles when mapped from the frequency deviation of 4.538 kHz. For example, as the tilt angle is 0 rad, the sensor's sensitivity is found to be 0.0007684 MHz/$\mu$rad (0.7684 GHz/rad), from which the tilt measurement uncertainty can be determined to be 6 $\mu$rad. Therefore, for different ranges of tilt angle, the performance of the present tilt sensor varies and needs to be carefully calibrated. The fundamental reason is the complicated dependence of the sensor's resonance frequency on the gap distance between the metal block and the open end of the coaxial line. However, for a relatively small range, e.g., 1 mrad, the response of the sensor is quite linear and consistent, as demonstrated in Fig. 5.

The influence of the initial setting of the gap distance $d$ between the endface of the mass block and the open end on the sensor device was also studied. Fig. 6 shows the response curves of the OE-HCCR inclinometer at three different initial settings of $d$. Note that the initial gap distances indicated in Fig. 6 were determined according to Fig. 2(b). As expected, the smaller the initial gap distance $d$, the larger the measurement sensitivity (i.e., decreases in resonance frequency per unit change in tilt angle). However, the dynamic range of the inclinometer decreased as the initial gap distance $d$ decreased. Thus, there is a tradeoff between the measurement sensitivity and dynamic range of the OE-HCCR-based inclinometer. Importantly, these findings demonstrated that the inclinometer is user-configurable, meaning that the dynamic range and measurement sensitivity can be flexibly adjusted for different applications. On the other hand, the zero-tilt point shown in the results was defined simply according to the readout from the 1-D tilt translation stage. Indeed, any point in the response curve of the sensor can be considered as the zero-tilt point such

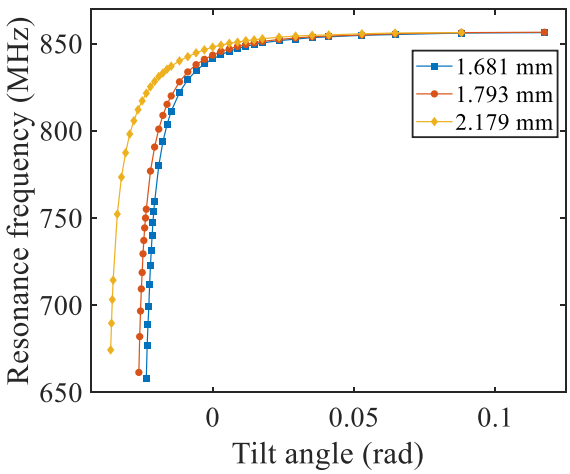


Fig. 6. Response curves of the OE-HCCR-based 1-D inclinometer device at three different initial settings of the gap distance $d$ between the open end and the endface of the mass block. The smaller the initial gap distance $d$, the larger the measurement sensitivity (i.e., decreases in resonance frequency per unit change in tilt angle).

that the dynamic range and sensitivity of the sensor for positive and negative tilt angle measurements can be flexibly adjusted. From another point of view, the sensitivity of the sensor is dependent on its initial resonance frequency; the smaller the resonance frequency, the higher the measurement sensitivity (i.e., the larger the slope).

### *B. 2-D Tilt Sensor*

In the calibration experiment for the 2-D tilt sensor, Port 1 and Port 2 of the VNA were used to interrogate the two OE-HCCRs simultaneously. The prototype device was mounted on the translation stage that was used for calibrating the 1-D sensor. The responses of the 2-D sensor device were evaluated by calibrating the responses for the two OE-HCCRs. Specifically, changes in tilt angle along the $x$-axis (see Fig. 3) were first applied to the 2-D sensor device, and responses from both OE-HCCRs were recorded. Subsequently, the device was rotated 90° and aligned so that tilt along the $y$-axis could be applied to the device for calibration of both OE-HCCRs for the orthogonal coordinate. The initial gap distances between the open end of OE-HCCR$_1$ and side face $M_1$ and the open end of OE-HCCR$_2$ and side face $M_2$ were adjusted to be approximately 2 mm. The two OE-HCCRs resonated at approximately 1.190 GHz at the initial settings. Fig. 7 presents the results of the 2-D prototype inclinometer device. Fig. 7(a) shows measured changes in the resonance frequencies of OE-HCCR$_1$ and OE-HCCR$_2$ as a function of applied tilt angles when the inclinometer was tilted along the $x$-axis. Fig. 7(b) shows the results when the tilt angles were applied along the $y$-axis. As can be seen from Fig. 7(a), the resonance frequency of OE-HCCR$_1$ decreased as the applied tilt angle decreased, which matched well with the 1-D device [see Fig. 4(c)]. Noticeable decreases in the resonance frequency of OE-HCCR$_2$ were also observed, which were attributed to $y-x$ crosstalk tilt errors. The $y-x$ crosstalk coefficient was determined to be 18.98 MHz/rad by means of linear curve fit to the measured data. As the tilt angle was applied along the $y$-axis direction, the resonance frequency of OE-HCCR$_2$ decreased as the applied tilt angle decreased,

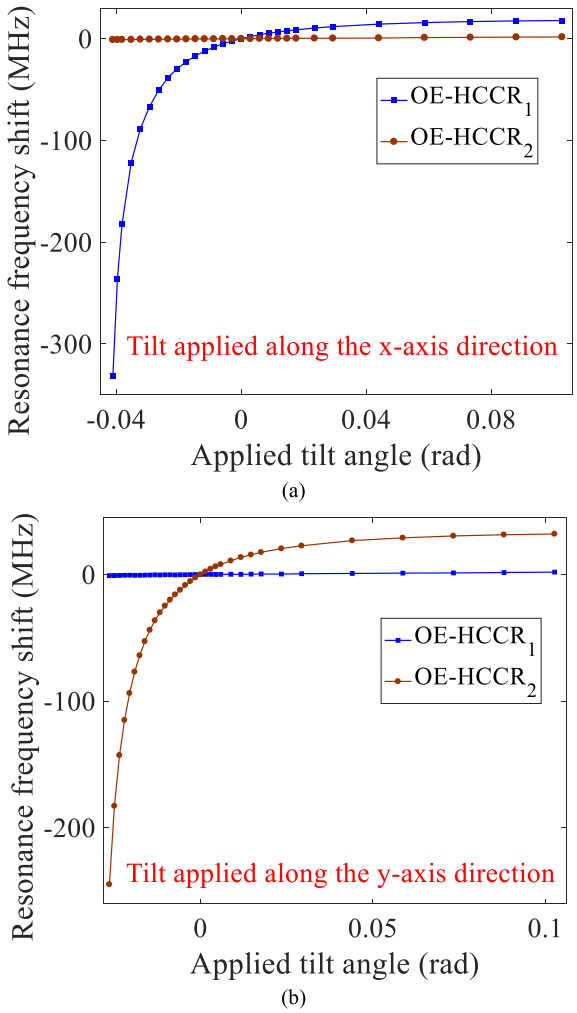


Fig. 7. Calibration experiment results for the prototype 2-D inclinometer device based on two OE-HCCR tilt sensors. (a) Plot of the resonance frequency shift of OE-HCCR$_1$ and OE-HCCR$_2$ as a function of tilt angles applied along the $x$-axis direction. The evolution of the resonance frequency shift for OE-HCCR$_1$ was expected and matched well with previous results. The resonance frequency shifts of OE-HCCR$_2$ versus applied tilt angles along the $x$-axis direction revealed a measured $y-x$ crosstalk coefficient of 18.98 MHz/rad. (b) Plot of the resonance frequency shift of OE-HCCR$_1$ and OE-HCCR$_2$ as a function of tilt angles applied along the $y$-axis direction. The resonance frequency shifts of OE-HCCR$_1$ versus applied tilt angles along the $y$-axis direction revealed a measured $x-y$ crosstalk coefficient of 20.34 MHz/rad.

as shown in Fig. 7(b), as expected. Similarly, decreases in resonance frequency up to several MHz were observed for OE-HCCR$_1$, attributed to $x-y$ crosstalk tilt errors. The $x-y$ crosstalk coefficient was determined to be 20.34 MHz/rad. The experimental results demonstrated that the prototype 2-D tilt sensor could be used for simultaneous tilt angle measurements in two orthogonal dimensions. Crosstalk errors between the two orthogonal dimensions (<1%) were observed in the experiments. The alignment errors introduced in the assembly of the prototype device and the fabrication errors of the device components primarily contributed to the measured crosstalk errors. For example, the open end of the OE-HCCR may not have been perfectly aligned parallel to the corresponding side face of the metal bar. As the inclinometer device was tilted along the $x$-axis, the gap distance between the open end of OE-HCCR$_2$ and $M_2$ slightly changed, resulting in resonance frequency shifts of OE-HCCR$_2$. Additionally, the experimental errors associated with one of the principal axes of the 2-D inclinometer device (i.e., $x$- or $y$-axes) not being positioned exactly parallel to the principal axis of the tilt translation stage may also have contributed to crosstalk errors. In that case, an additional orthogonal component of tilt angle would be introduced and metered by the 2-D inclinometer device as the device was tilted in the 1-D calibration experiment.

## IV. Conclusion

An OE-HCCR-based inclinometer device for tilt angle measurements with a resolution of 110 nrad was demonstrated. The basic idea of the sensor design was to combine an ultrasensitive OE-HCCR with a pendulum structure that served as the tilt-sensitive element. A cylindrical metal mass block was suspended in proximity and parallel to the open end of the resonator using two nylon ropes. When the sensor device was tilted, due to a judicious mechanical design, the distance between the open end and the endface of the mass block changed, resulting in a resonance frequency shift of the OE-HCCR. By tracking the frequency shift, the OE-HCCR-based device could be used as an inclinometer after proper calibration. In the demonstration experiments, the dynamic range of the device was studied. The responses of the inclinometer to small changes in tilt angles were also demonstrated, showing a measurement resolution of 110 nrad over a dynamic range of 3.75 mrad. Importantly, the dynamic range and measurement sensitivity of the inclinometer could be easily adjusted by changing the initial setting of the gap distance between the open end and the mass block, which was also experimentally verified. Moreover, the dynamic range and measurement sensitivity of the inclinometer device could also be adjusted by changing the lengths of the suspending ropes. Additionally, based on the 1-D sensor, a 2-D prototype inclinometer device for simultaneous measurements of changes in tilt angles in two orthogonal directions was fabricated and demonstrated. Note that although a two-port VNA was used in the demonstration experiment, a low-cost one-port VNA can be used as the interrogator for the 1-D sensor and together with an electronic switch for interrogating the 2-D sensor. The system cost can be further reduced by building the bespoke electronics since only the reflection spectrum in magnitude is needed for sensing applications.

The demonstrated OE-HCCR inclinometers hold the advantages of high measurement resolution, robustness, cost-effectiveness, ease of compact fabrication, and user-configurable capability. It is envisioned that the compact novel inclinometer device could be deployed in large numbers for measurements at multiple spatially disposed points for SHM, solid Earth tide studies, and for forecasting natural disasters (e.g., earthquakes and landslides). The fundamental strategy behind the present tilt sensor, i.e., the combination of a high-sensitivity microwave sensing technology with a conventional mechanical transducer, is highly generalizable, from which a new generation of ultrasensitive, low-cost, and robust microwave sensors is expected to be developed for potential industrial applications.

## Acknowledgment

Jie Huang is grateful for support from the Roy A. Wilkens Professorship Endowment.

## REFERENCES


[1] J. A. C. Horsfall and G. C. P. King, "A new geophysical tiltmeter," *Nature*, vol. 274, no. 5672, pp. 675–676, Aug. 1978.

[2] H. Tsuruoka, M. Ohtake, and H. Sato, "Statistical test of the tidal triggering of earthquakes: Contribution of the ocean tide loading effect," *Geophys. J. Int.*, vol. 122, no. 1, pp. 183–194, Jul. 1995.

[3] M. Bouchon and K. Aki, "Strain, tilt, and rotation associated with strong ground motion in the vicinity of earthquake faults," *Bull. Seismol. Soc. Amer.*, vol. 72, no. 5, pp. 1717–1738, Oct. 1982.

[4] S. Wu, S. Fan, J. Luo, and H. Hsu, "Folded pendulum tiltmeter," *Rev. Sci. Instrum.*, vol. 73, no. 5, pp. 2150–2156, May 2002.

[5] Q. Han and C. Chen, "Research on tilt sensor technology," in *Proc. IEEE Int. Symp. KAM*, Dec. 2008, pp. 786–789.

[6] Z. Chen, G. Hefferman, L. Yuan, Y. Song, and T. Wei, "Terahertz-range interrogated grating-based two-axis optical fiber inclinometer," *Opt. Eng.*, vol. 55, no. 2, 2016, Art. no. 026106.

[7] J. S. Bajić, D. Z. Stupar, L. M. Manojlović, M. P. Slankamenac, and B. M. Živanov, "A simple, low-cost, high-sensitivity fiber-optic tilt sensor," *Sens. Actuators A, Phys.*, vol. 185, pp. 33–38, Oct. 2012.

[8] H. Y. Au, S. K. Khijwania, H. Y. Fu, W. H. Chung, and H. Y. Tam, "Temperature-insensitive fiber Bragg grating based tilt sensor with large dynamic range," *J. Lightw. Technol.*, vol. 29, no. 11, pp. 1714–1720, Jun. 1, 2011.

[9] H. Bao, X. Dong, L.-Y. Shao, C.-L. Zhao, C. C. Chan, and P. Shum, "Temperature-insensitive 2-D pendulum clinometer using two fiber Bragg gratings," *IEEE Photon. Technol. Lett.*, vol. 22, no. 12, pp. 863–865, Jun. 15, 2010.

[10] B.-J. Peng, Y. Zhao, Y. Zhao, and J. Yang, "Tilt sensor with FBG technology and matched FBG demodulating method," *IEEE Sensors J.*, vol. 6, no. 1, pp. 63–66, Feb. 2006.

[11] B. O. Guan, H. Y. Tam, and S. Y. Liu, "Temperature-independent fiber Bragg grating tilt sensor," *IEEE Photon. Technol. Lett.*, vol. 16, no. 1, pp. 224–226, Jan. 2004.

[12] H. Bao, X. Dong, L.-Y. Shao, C.-L. Zhao, and S. Jin, "Temperature-insensitive 2-D tilt sensor by incorporating fiber Bragg gratings with a hybrid pendulum," *Opt. Commun.*, vol. 283, pp. 5021–5024, Dec. 2010.

[13] D. Inaudi and B. Glisic, "Development of a fiber optic interferometric inclinometer," *Proc. SPIE*, vol. 4694, pp. 36–43, Jun. 2002.

[14] S. Liu, N. Liu, M. Hou, J. Guo, Z. Li, and P. Lu, "Direction-independent fiber inclinometer based on simplified hollow core photonic crystal fiber," *Opt. Lett.*, vol. 38, no. 4, pp. 449–451, Feb. 2013.

[15] Y. Zhuang, Y. Chen, C. Zhu, R. E. Gerald, and J. Huang, "Probing changes in tilt angle with 20 nanoradian resolution using an extrinsic Fabry–Pérot interferometer-based optical fiber inclinometer," *Opt. Exp.*, vol. 26, no. 3, pp. 2546–2558, Feb. 2018.

[16] J. N. Munday and W. M. Robertson, "Slow electromagnetic pulse propagation through a narrow transmission band in a coaxial photonic crystal," *Appl. Phys. Lett.*, vol. 83, no. 5, pp. 1053–1055, Aug. 2003.

[17] T. Wei, S. Wu, J. Huang, H. Xiao, and J. Fan, "Coaxial cable Bragg grating," *Appl. Phys. Lett.*, vol. 99, no. 11, Sep. 2011, Art. no. 113517.

[18] S. Wu, T. Wei, J. Huang, H. Xiao, and J. Fan, "Modeling of coaxial cable Bragg grating by coupled mode theory," *IEEE Trans. Microw. Theory Techn.*, vol. 62, no. 10, pp. 2251–2259, Oct. 2014.

[19] J. Huang, T. Wang, L. Hua, J. Fan, H. Xiao, and M. Luo, "A coaxial cable Fabry–Pérot interferometer for sensing applications," *Sensors*, vol. 13, no. 11, pp. 15252–15260, Nov. 2013.

[20] C. Zhu, Y. Chen, Y. Zhuang, and J. Huang, "A centimeter-range displacement sensor based on a hollow coaxial cable Fabry–Pérot resonator," *IEEE Sensors J.*, vol. 18, no. 11, pp. 4436–4442, Jun. 2018.

[21] C. Zhu, Y. Zhuang, Y. Chen, and J. Huang, "A liquid-level sensor based on a hollow coaxial cable Fabry–Pérot resonator with micrometer resolution," *IEEE Trans. Instrum. Meas.*, vol. 67, no. 12, pp. 2892–2897, Dec. 2018.

[22] C. Zhu, Y. Chen, Y. Zhuang, and J. Huang, "Displacement and strain measurement up to 1000 °C using a hollow coaxial cable Fabry–Pérot resonator," *Sensors*, vol. 18, no. 5, p. 1304, Apr. 2018.

[23] C. Zhu, Y. Zhuang, Y. Chen, and J. Huang, "A hollow coaxial cable Fabry–Pérot resonator for liquid dielectric constant measurement," *Rev. Sci. Instrum.*, vol. 89, no. 4, Apr. 2018, Art. no. 045003.

[24] C. Zhu, Y. Zhuang, Y. Chen, B. Zhang, and J. Huang, "Contactless liquid interface measurement based on a hollow coaxial cable resonator," *Sens. Actuators A, Phys.*, vol. 285, pp. 623–627, Jan. 2019.

[25] M. A. Stuchly and S. S. Stuchly, "Coaxial line reflection methods for measuring dielectric properties of biological substances at radio and microwave frequencies—A review," *IEEE Trans. Instrum. Meas.*, vol. IM-29, no. 3, pp. 176–183, Sep. 1980.

[26] A. L. Gioia *et al.*, "Open-ended coaxial probe technique for dielectric measurement of biological tissues: Challenges and common practices," *Diagnostics*, vol. 8, no. 2, p. 40, Jun. 2018.

[27] P. De Langhe, L. Martens, and D. De Zutter, "Design rules for an experimental setup using an open-ended coaxial probe based on theoretical modelling," *IEEE Trans. Instrum. Meas.*, vol. 43, no. 6, pp. 810–817, Dec. 1994.

[28] T. W. Athey, M. A. Stuchly, and S. S. Stuchly, "Measurement of radio frequency permittivity of biological tissues with an open-ended coaxial line: Part I," *IEEE Trans. Microw. Theory Techn.*, vol. MTT-30, no. 1, pp. 82–86, Jan. 1982.

[29] J. R. Mosig, J.-C.-E. Besson, M. Gex-Fabry, and F. E. Gardiol, "Reflection of an open-ended coaxial line and application to nondestructive measurement of materials," *IEEE Trans. Instrum. Meas.*, vol. IM-30, no. 1, pp. 46–51, Mar. 1981.

[30] P. M. Meaney, A. P. Gregory, J. Seppälä, and T. Lahtinen, "Open-ended coaxial dielectric probe effective penetration depth determination," *IEEE Trans. Microw. Theory Techn.*, vol. 64, no. 3, pp. 915–923, Mar. 2016.

[31] M. Hussein, F. Awwad, D. Jithin, H. E. Hasasna, K. Athamneh, and R. Iratni, "Breast cancer cells exhibits specific dielectric signature *in vitro* using the open-ended coaxial probe technique from 200 MHz to 13.6 GHz," *Sci. Rep.*, vol. 9, no. 1, pp. 1–8, Mar. 2019.

[32] V. Guihard, F. Taillade, J.-P. Balayssac, B. Steck, J. Sanahuja, and F. Deby, "Permittivity measurement of cementitious materials with an open-ended coaxial probe," *Construct. Building Mater.*, vol. 230, Jan. 2020, Art. no. 116946.

[33] S. A. Komarov, A. S. Komarov, D. G. Barber, M. J. L. Lemes, and S. Rysgaard, "Open-ended coaxial probe technique for dielectric spectroscopy of artificially grown sea ice," *IEEE Trans. Geosci. Remote Sens.*, vol. 54, no. 8, pp. 4941–4951, Aug. 2016.

[34] C. L. Brace and S. Etoz, "An analysis of open-ended coaxial probe sensitivity to heterogeneous media," *Sensors*, vol. 20, no. 18, p. 5372, Sep. 2020.

[35] E. Tanabe and W. T. Joines, "A nondestructive method for measuring the complex permittivity of dielectric materials at microwave frequencies using an open transmission line resonator," *IEEE Trans. Instrum. Meas.*, vol. IM-25, no. 3, pp. 222–226, Sep. 1976.

[36] D. Xu, L. Liu, and Z. Jiang, "Measurement of the dielectric properties of biological substances using an improved open-ended coaxial line resonator method," *IEEE Trans. Microw. Theory Techn.*, vol. MTT-35, no. 12, pp. 1424–1428, Dec. 1987.

[37] S. Kono, H. Imamura, and K. Nakagawa, "Non-destructive monitoring of food freezing process by microwave resonance spectroscopy with an open-ended coaxial resonator," *J. Food Eng.*, vol. 292, Mar. 2021, Art. no. 110293.

[38] C. Zhu, R. E. Gerald, and J. Huang, "Highly sensitive open-ended coaxial cable-based microwave resonator for humidity sensing," *Sens. Actuators A, Phys.*, vol. 314, Oct. 2020, Art. no. 112244.

[39] C. Zhu, R. E. Gerald, Y. Chen, and J. Huang, "Metal-organic framework portable chemical sensor," *Sens. Actuators B, Chem.*, vol. 321, Oct. 2020, Art. no. 128608.

[40] C. Zhu, R. E. Gerald, and J. Huang, "Microwave device inspired by fiber-optic extrinsic Fabry–Pérot interferometer: A novel ultra-sensitive sensing platform," *J. Lightw. Technol.*, vol. 38, no. 24, pp. 6961–6966, Dec. 15, 2020.

[41] C. Zhu, R. E. Gerald, Y. Chen, and J. Huang, "Probing the theoretical ultimate limit of coaxial cable sensing: Measuring nanometer-scale displacements," *IEEE Trans. Microw. Theory Techn.*, vol. 68, no. 2, pp. 816–823, Feb. 2020.